Dalton Transactions

Accepted Manuscript

ROYAL SOCIETY OF CHEMISTRY

www.rsc.org/dalton

Luminescent Pt(II) Complexes Bearing Dual Isoquinolinyl Pyrazolates: Fundamentals and Applications

Hsiao-Yun Ku,[a] Bihai Tong,[a,b] Yun Chi,*[,a] Hao-Che Kao,[c] Chia-Chi Yeh,[c] Chih-Hao Chang,[c,*] Gene-Hsiang Lee,[d]

[a] Department of Chemistry, National Tsing Hua University, Hsinchu 30013, Taiwan; E-mail: ychi@mx.nthu.edu.tw

[b] College of Metallurgy and Resources, Institute of Molecular Engineering and Applied Chemistry, Anhui University of Technology, Ma'anshan, Anhui 243002, China

[c] Department of Photonics Engineering, Yuan Ze University, Chungli 32003, Taiwan; E-mail: chc@saturn.yzu.edu.tw

[d] Department of Chemistry and Instrumentation Center, National Taiwan University, Taipei 10617, Taiwan

TOC Illustration:

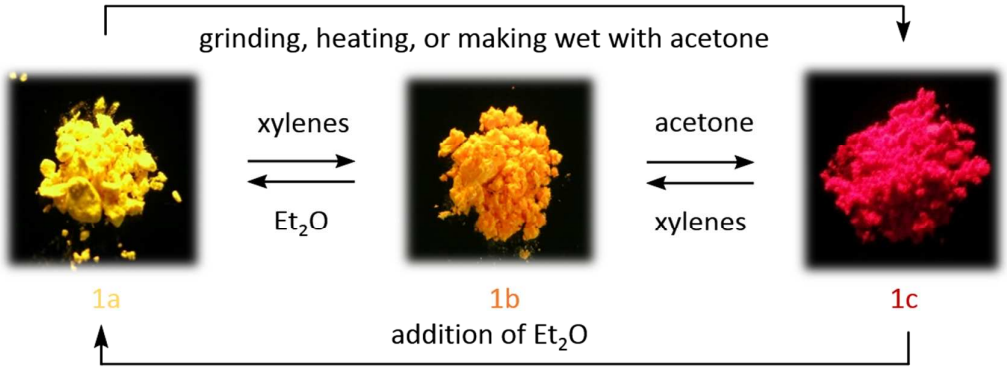

Pt(II) complex [Pt(L*x*)$_2$], L*x*H = 6-*t*-butyl-1-(3-trifluoromethyl-1H-pyrazol-5-yl) isoquinoline, with three colored morphologies can be interconverted by grinding and/or making wet with solvents.

Abstract

A series of four Pt(II) metal complexes with *trans*-arranged isoquinolinyl azolates have been prepared, $[Pt(Lx)_2]$, x = 1 ~ 4, (**1** ~ **4**). The associated chelates possess various substituents; namely: one *t*-butyl (Bu^t) at the 6-position (L1), two Bu^t groups at the 5,7-positions (L2), one dip (2,6-di-isopropylphenyl) group at the 6-position (L3), and single dip group at the 4-position of the 1-isoquinolinyl fragment (L4), respectively. Crystal structures of **1** and **4** were determined to shed light on the relationship of photophysics and packing arrangements. Their photophysical properties were measured and compared, for which the solid-state emission spectra of **2** and **4** are nearly identical to the solution spectra of all Pt(II) complexes, showing formation of isolated molecular entities. In contrast, Pt(II) complexes **1** and **3** are found to be sensitive to their morphological states and external stimulus. This is confirmed by the gradual red-shifting of emission with increasing concentration in PMMA matrix, and eventual formation of the broadened, metal–metal-to-ligand charge transfer (MMLCT) emission, by (i) making wet with acetone and drying in air, or (ii) grinding with mortar and pestle, respectively. Organic light emitting diodes (OLEDs) were also fabricated using multiple layered architecture and lowered doping concentration (e.g. 8 wt.%), the latter is for avoiding the dopant aggregation in the emitting layer. The associated OLED performances (i.e. η_{max} = 11.5 %, 8.5%, and 11.2% for **1**, **2** and **3**) confirmed their suitability and potential as dopant for phosphorescent OLEDs.

Third-row, late transition metal complexes with either d^6 or d^8-electronic configuration are known to have strong spin-orbit coupling (SOC) exerted by the central metal atom, which then induced a fast intersystem crossing between the single and triplet excited states and afforded bright phosphorescence in both fluid and solid phases at RT.[1] Then, the higher emission efficiency triggered extensively investigation on their applications as dopant emitters in the organic light-emitting diode (OLEDs), for which the effective harvesting of all excitons is expected to give a unitary internal quantum efficiency.[2] Hence, their syntheses, photophysical studies and applications were extensively elaborated during the past two decades. Parallel to this research endeavor, the needs for efficient OLED emitters have promoted studies on the luminescent Pt(II) phosphors.[3] In contrast to the d^6-metal phosphors, Pt(II) complexes adopt the square planar geometries due to the d^8-electronic configuration. Formation of excimer (or exciplex) upon excitation has been observed and explained using associated bonding theory and consideration of their ground state structures.

Moreover, the ππ-stacking interaction between the square-planar Pt(II) complexes would promote formation of the so-called, metal–metal-to ligand charge transfer (MMLCT) transition,[4] which is substantially red-shifted compared with the typical emission caused by the combined ligand-centered ππ* and metal-to-ligand charge transfer (MLCT) excited states. Hence, partial formation of MMLCT emission at longer wavelength may allow generation of dual phosphorescence for the Pt(II) based dopants and offer an easy access of the single dopant, white light-emitting OLEDs (WOLEDs).[5] Alternatively, functionalized tetradentate chelates, with incorporation of bulky ancillaries, were employed to modify the coordination environment and to suppress the intermolecular interactions.[6] With these endeavors, a leaping progression in the fabrication of efficient phosphorescent OLEDs with different visual colors were reported in the literature.

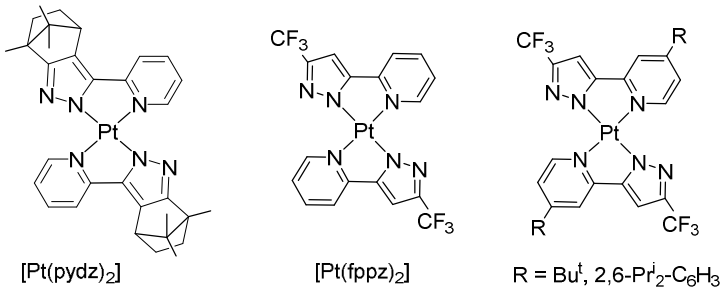

Chart 1. Structural drawing of Pt(II) complexes bearing selected functional pyrazolate chelates.

Recently, we have worked on the Pt(II) phosphors bearing 5-pyrid-2-yl azolates (both pyrazolate and triazolate) and analogous indazolates, cf. Chart 1.[7] Variation of the π-conjugation, steric encumbrance, substitution pattern and internal electronic characteristics of the corresponding chelates were systematic varied in turning of the emission color.[8] Moreover, some of these Pt(II) complexes with electron deficient ligating fragments have also showed strong tendency to aggregate in solid states,[9] giving the MMLCT transition at longer wavelength region. For probing this property, we now focused on the synthesis, characterization, and photophysics of Pt(II) complexes **1** – **4** with tailor-made isoquinolinyl azolates (Chart 2), for which their fused aromatic skeletons are expected to exhibit both greater π-conjugation and stronger intermolecular ππ-stacking interaction versus the smaller pyridyl analogues and, in turn, to afford distinctive photophysics and spectral dependence based on the number and position of substituents.[10] Hence, the recorded photophysical responses and device performance would be of valuable in revising future design of Pt(II) phosphors, particularly under the condition that complex **1** has already showed higher efficiency as dopant of monochrome OLEDs and white-emitting OLEDs.

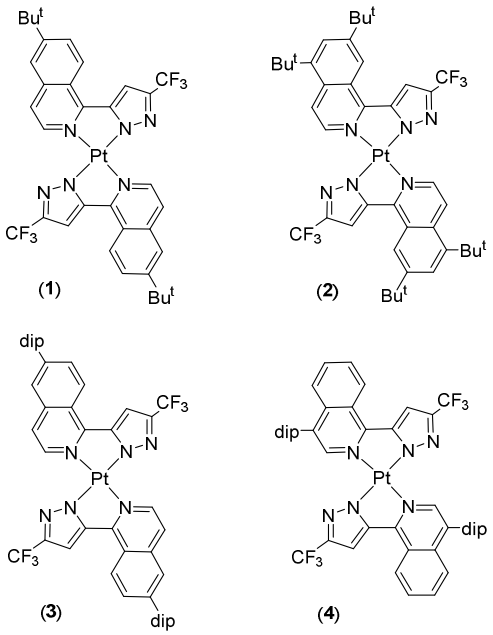

Chart 2. Structural drawing of the studied Pt(II) complexes; dip = 2,6-di-isopropylphenyl.

Results and Discussion

Synthesis and Characterization. The pyrazolic chelates are obtained from multi-step syntheses initiated from the substituted isoquinoline precursors. For record tracking, 4-bromoisoquinoline was obtained from commercial supplier, while other isoquinolines, namely: 6-bromoisoquinoline, 6-*t*-butyl-isoquinoline and 5,7-di-*t*-butyl-isoquinoline, were synthesized from aminoacetaldehyde dimethyl acetal and respective aromatic aldehydes using Pomeranz-Fritsch reaction.[11] The subsequent acetylation of isoquinolines was achieved employing para-acetaldehyde, *t*-BuO_2H, trifluoroacetic acid and $FeSO_4 \cdot 7H_2O$.[12] Next, the 1-acetyl-4-*t*-butyl and 1-acetyl-5,7-di-*t*-butyl isoquinolines were employed for the preparation of pyrazole chelate L1 and L2 using Claisen condensation and hydrazine cyclization,[13] while the 1-acetyl-4-bromoisoquinoline and 6-bromoisoquinoline were reacted with 2,6-diisopropylphenylboronic acid to afford the respective 2,6-diisopropylphenyl substituted isoquinolines. The isoquinolinyl pyrazoles, L3 and L4, were obtained by

similar protocol. Schematic synthetic procedures are depicted in Scheme 1, while detailed procedures are given in the Electronic Supporting Information.

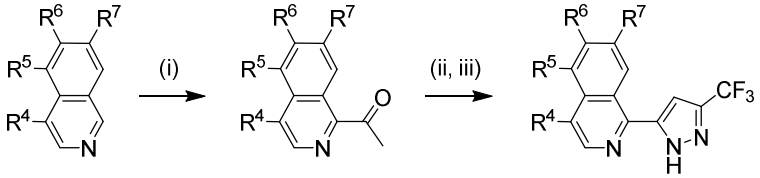

L1: $R^6 = Bu^t$; L2: $R^5 = R^7 = Bu^t$; L3: R^6 = dip; L4: R^4 = dip

Scheme 1. Synthetic procedures for L1 ~ L4, dip = 2,6-diisopropylphenyl; experimental conditions: (i) $FeSO_4 \cdot 7H_2O$, acetaldehyde, *t*-BuO_2H and CF_3CO_2H, (ii) CF_3CO_2Et, NaH, THF, (iii) N_2H_4, EtOH.

The isoquinolinyl pyrazolate Pt(II) complexes **1** – **4**, having the general formula $[Pt(Lx)_2]_2$, *x* = 1 ~ 4, (Chart 2) were next synthesized from reaction of $[PtCl_2(DMSO)_2]$ with two equiv. of the aforementioned pyrazole ligand L1 ~ L4 in presence of Na_2CO_3 and THF solvent. It was observed that the Pt(II) complexes **1** ~ **3** were precipitated out of the solution even during the reflux, as they are only sparingly soluble in THF. The only exception is the Pt(II) complex **4** with 4-dip-substituted isoquinoline, which showed good solubility in THF, as well as in other common organic solvents such as acetone, toluene and CH_2Cl_2. The higher solubility may be associated with the weakened ππ-stacking interaction between the planar Pt(II) complexes in solid state. On the other hand, the 6-*t*-butyl and dip substituents (i.e. in **1** and **3**), and the 5,7-di-*t*-butyl substituents (i.e. in **2**) are not bulky enough in effectively blocking the intermolecular ππ-stacking interaction versus the single 4-dip-substituent in Pt(II) complex **4** and, therefore, are found to be less soluble.

Characterization was first conducted using mass spectrometry and ^1H NMR spectroscopy. The Pt(II) complexes **1**, **2** and **4** are soluble in $CDCl_3$, while complex **3** requires the use of d_8-THF for achieving adequate solubility. All ^1H NMR spectra showed a characteristic signal at δ 10.76 ~ 10.50 due to the CH unit next to the N

atom of isoquinolinyl fragment. The downfield shifting is caused by the inter-ligand C-H···N hydrogen bonding, as shown in the related Os(II) complexes.[14]

The Pt(II) metal complexes **1** and **4** were also examined by single-crystal X-ray diffraction analysis to establish their molecular structure and the associated intermolecular interaction. Figure 1a shows the structural drawing of one representative molecule of Pt(II) complex **1**. The av. Pt-N bond length to the pyrazolate fragment (2.01(1) Å) in **1** is shorter than those of the av. Pt-pyridine distance (Pt-N = 2.034(7) Å). This difference is consistent with the stronger Pt-N bonding interaction to the pyrazolates versus that of the neutral pyridine fragments. In fact, the observed metric data are akin to those observed for relevant Pt(II) complexes,[8c, 8e, 15] for which the av. Pt-N distance to azolate and pyridine fragments is measured to be ~1.98 Å and ~2.02 Å, while small variations can be attributed to the electronic effects of chelates.

Figure 1b showed the crystal packing diagram, in which Pt(II) complex **1** exhibited a trimeric packing motif, characterized by the existence of two identical and shortened Pt···Pt non-bonding contacts of 3.338 Å. The central Pt(II) molecule is rotated by ~40° alone the Pt-Pt-Pt axis for making enough of room to accommodate the *t*-butyl substituents of the chelates. Moreover, a Pt···Pt contact of 5.197 Å, which is substantially longer than the non-bonding Pt···Pt contact reported in literature,[16] together with the co-existence of xylene solvates, defined the boundary to the proposed Pt_3 stacking units. It is notable that its parent pyridyl pyrazolate complex *trans*-$Pt(pyzpy)_2$, Hpyzpy = 2-(1H-pyrazol-3-yl)pyridine, also crystallizes in units of three parallel stacked Pt(II) molecules separated by ~3.30 Å,[17] forming the perpendicularly arranged trimer, not the slipped trimer as observed in the present system. DFT calculation also confirmed that the *trans*-$Pt(pyzpy)_2$ trimer is energetically more favorable over other packing structures, providing the theoretical account for its existence.[17]

Next, the structural analysis of Pt(II) complex **4** with 4-dip substituents was also

conducted to offer a direct comparison between the packing arrangement of Pt(II) complex **1** that showed notable ππ-stacking interaction. As illustrated in Figure 2, the gross molecular arrangement and the corresponding Pt-N distances (Pt(1)-N(1) = 2.040(4) and Pt(1)-N(2) = 1.998(4) Å) are both akin to those of aforementioned Pt(II) complex **1**, on which the dip substituents are residing perpendicular to the Pt(II) core framework, for achieving minimal steric interference. As for the Pt(II) molecules, they are aligned in a tilted stacking and with an elongated Pt···Pt contact of 8.828 Å. Thus, this packing alignment can be employed to account for the higher solubility in solution as well as the possession of identical emission spectra in both solution and solid states (vide infra).

Photophysical Properties. Figure 3 depicts UV-Vis absorption and emission spectra of Pt(II) metal complexes **1 – 4** in CH_2Cl_2 at RT, while numerical data are summarized in Table 1. As expected, their absorption spectra can be understood and ascribed to several domains in terms of the absorption intensities. First, the higher-energy region (< 380 nm) with extinction coefficients greater than 10^4 $M^{-1}cm^{-1}$ is attributed to the ligand-centered ππ* pyrazolate → isoquinoline transitions. This assignment is supported by the similar electronic transition observed for other Pt(II) complexes.[18] On the other hand, the lower-energy bands with relatively small extinction coefficients around 380 – 450 nm (ca. 7700 ~ 4700 $M^{-1}cm^{-1}$) can then be assigned to the metal-to-ligand charge-transfer band (MLCT) mixed with a substantial degree of ligand-centered ππ* transition.[19] Moreover, all complexes **1 – 4** exhibit identical spectral profile, indicating the existence of solvated species, all with essentially identical core structure. This information is particular important as complex **4** showed no possession of both aromatic ππ and Pt···Pt stacking interaction according to the X-ray structural data (i.e. devoid of ground state dimer or higher oligomers), while single dip-substituted Pt(II) complex **3** and the *t*-butyl substituted complex **1** are relatively insoluble and exhibited notable solvato- and mechanoluminescence in solid form, respectively. These properties, plus the

concentration-dependent luminescence detected in poly(methyl methacrylate) PMMA (vide infra), are obviously caused by the solid-state aggregation imposed by the planar morphologies.

Furthermore, all samples show strong yellow emission in degassed solution at RT with quantum yield in the range from 21% to 34% for **1** – **4**, respectively. The notable vibronic splitting and the long emission lifetime (τ_{obs} = 15.5 ~ 26.1 μs) indicated the greater contribution from the $^3\pi\pi$-excited states.[20] The first emission peak maxima ($E_{0\text{-}0}$) follows an order of **1** ~ **3** (~ 563 nm) < **2** ~ **4** (~ 574 nm), meaning that the 6-*t*-butyl and 6-dip substituents in both **1** and **3** are capable of enlarging the emission energy gap versus that of Pt(II) complexes **2** and **4** bearing the 5,7-di-*t*-butyl and 4-dip substituents on chelates. Moreover, the nearly identical emission profile indicated the lack of excimer and excited state dimer or higher aggregate in solution, which is in accordance to the UV-Vis spectral measurements.

The solid-state emission spectra were also measured to reveal the possible difference versus those observed in solution. First, Pt(II) complexes **2** and **4** revealed identical spectral pattern, which is consistent with their higher solubility in typical organic solvents and the lack of notable ππ-stacking interaction in solid as revealed by X-ray study on **4**. Figures S1 and S2 of supporting information exhibited the normalized emission spectra of **2** and **4** recorded in CH_2Cl_2 solution and as neat powder. The slight variation in their peak positions is probably attributed to the change of recording media, for which the neat powder is expected to possess a more rigid environment and forfeit solvation versus that recorded in CH_2Cl_2 solution.[21]

In sharp contrast, the solid-state emission for Pt(II) complex **1** obtained after making wet with diethyl ether (or hexane, CH_2Cl_2 and ethyl acetate), showed similar color and spectral pattern (with three maxima at 561, 604 and 658 nm) versus that recorded in CH_2Cl_2 solution (Figures 4 and 5), indicating the retention of isolated molecules (cf. 1a). However, after making wet with aromatic solvent such as xylenes (or toluene and chlorobenzene), the corresponding spectrum underwent a slightly

red-shifting and gave three peak maxima at 582, 622 and 680 nm (cf. 1b), which are fully consistent with the formation of trimeric excimer (or other type of excimer) in crystalline state. Furthermore, upon making wet with acetone, the emission turned to a broad and featureless profile with peak maximum at 656 nm (cf. 1c). This feature is akin to Pt(II) complexes with severe aggregation in solid states, particularly to those with one-dimensional, infinite chain-like stacking arrangement.[22] Thus, we can confidently assign this lowest energy emission to the metal–metal-to-ligand charge transfer transition (MMLCT),[4a-4e] for which the packing arrangement is probably switching from the single Pt(II) complex and/or Pt_3 trimer to the infinite metal chain-like structure that is stabilized by formation of chain-like Pt···Pt interaction after making wet with acetone. Moreover, formation of red-emitting solid can be also achieved using solvents such as THF, $CHCl_3$, DMF and methanol, respectively, confirming its link to the solvent polarity in altering the stacking interaction in solid state.

Beside the remarkable response to the solvents, Pt(II) complex **1** also showed higher sensitivity to the mechanical perturbation.[23] Figure 6 showed photographic images of **1** in response to mechanical grinding and addition of solvent. As can be seen, grinding with mortar and pestle has crushed yellow solid to red-orange powder, both in ambient and under UV irradiation. Naturally, the applied mechanical stimuli has forced the Pt(II) complex **1** to align in the parallel arrangement, giving formation of substantial and direct Pt···Pt contact.[24] On the other hand, addition of diethyl ether has restored the loosed packing arrangement and changed the emission back to yellow.

We also disperse Pt(II) complex **1** into the PMMA matrix for studying the luminescence in response to the concentration. As shown in Figure S3 of supporting information, at the doping level of 1 wt.%, the emission profile is almost identical to that recorded in CH_2Cl_2 solution at RT, showing the existence of discrete molecule. Upon increasing the doping level up to 50 wt.%, the 0-0 peak is gradually

disappearing, together with a slow emergence for a featureless band with new maximum at 645 nm, which could be due to the co-existence of both discrete molecule and aggregated oligomer in varied proportion. However, this new band is found to be located in the higher energy region compared with that of the neat powder centered at 656 nm, for which this small difference could be attributed to the higher rigidity and varied electronic influence of PMMA media. Furthermore, formation of the trimer, its existence has been indicated by X-ray structural study of **1**, cannot be confirmed in this series of measurement due to the severe broadening of emission profile.

We also investigated the solid state emission spectra of Pt(II) complex **3**, which is related to **1** by replacing its 6-*t*-butyl substituent with an even more bulky dip substituent. Therefore, we anticipate to see photophysical effect caused by the reduced intermolecular interaction. To our surprise, the neat powder of **3** showed featureless emission profile with maxima centered at 655 nm and 729 nm after making wet with diethylether or THF, respectively (Figure 7). Both spectra are substantially red-shifted compared with the spectrum recorded in CH_2Cl_2, and even the solid state spectra of **1** under treatments such as addition of acetone, and grinding with mortar and pestle. Naturally, it can be assigned to the formation of excimer and/or higher order of aggregation,[25] but this deduction seems to be quite unlikely at the first glance. This is due to the fact that the individual Pt(II) unit in **1** must rotate by approx. 40° along the Pt···Pt axis to form the observed Pt_3 trimer, as revealed by the X-ray structural data. As a consequence, this freedom in making adjustment in solid will direct the dip substituents to stay away from each other and give reduced steric interference between the arrays of Pt(II) molecules. After then, the stronger electron withdrawing character of dip-substituents may also come into action, lowering the LUMO and giving further red-shifted emission versus that of **1** under similar conditions.

OLED Device Fabrication. Pt(II) complexes **1** ~ **3** were selected as dopants for fabrication of OLEDs. A host with a wider triplet energy gap is needed to prevent a reverse energy transfer from the triplet emitters to the host material.[26] Furthermore, bipolar host materials are preferable, as their better carrier transport capability is expected to enlarge recombination zone and give reduction of local concentration of excitons in the emitting layer (EML).[27] Thus, both the triplet-triplet and triplet-polaron (charged molecules) annihilation can be suppressed.[28] Considering these requirements, 4,4'-bis(carbazol-9-yl)biphenyl (CBP), was chosen as the host material of EML due to its bipolar capability as well as higher triplet energy gap (E_T) of 2.56 eV, and good hole and electron mobilities of 3.8×10^{-4} and 4.4×10^{-4} $cm^2 \cdot V^{-1} \cdot s^{-1}$, respectively.[29] Di-[4-(N,N-ditolyl-amino)-phenyl]cyclohexane (TAPC) was employed as the hole transporting material, for its higher triplet gap of ~2.8 eV, higher mobility, and a low LUMO which can be used to block excessive electron injection.[30] The device was then completed using 3,3',5,5'-tetra[(m-pyridyl)-phen-3-yl]biphenyl (BP4mPy) as the electron-transport layer to ensure effective exciton confinement.[31] As such, the generalized device architecture is indicated as follows: ITO/TAPC (40 nm)/CBP doped with 8 wt.% of Pt complex (30 nm)/BP4mPy (40 nm)/LiF (0.8 nm)/Al (150 nm).[32] Figure 8 depicted the structural drawings of these employed materials and schematic architecture of tested OLEDs.

Moreover, Figure 9 and Table 2 showed the electroluminescence (EL) characteristics and associated numerical data of the devices employing Pt(II) dopants **1** ~ **3**. As depicted in Figure 9(a), all OLED devices display an EL spectrum with notable vibronic fine structure similar to their solution photoluminescence, implying the carrier recombination is mainly occurred at the Pt(II) dopant within the EML of the device.[33] The full width at half maximum (FWHM) and other extracted PL and EL characteristics were summarized in Table 3. As can be seen, the EL spectra were red-shifted by about 2 to 10 nm versus their PL spectra, among which the device B

(i.e. **2**) showed the least red-shifted EL spectra (i.e. 2 nm), consistent with the lack of significant ππ-stacking interaction in solid-state. Moreover, the FWHM of all EL spectra were 20 ~ 30 nm wider than that of their individual PL spectrum. This could be due to the influence of media, and co-existence of monomer emission and a lower proportion of the ^{3}MMLCT emission from excimer, dimer and/or higher oligomer.[25]

The current density-voltage-luminance (*J-V-L*) diagrams showed that the current density follows the descending sequence: A > C > B (Figure 9(b)). At the driving voltage of 10 V, the current density was recorded to be 850, 765 and 710 mA·cm^{-2} for devices A, C, and B, respectively. Since all complexes **1** ~ **3** have similar emission energy gap, and the current density of device B (i.e. **2**) is much lower than that of devices A (i.e. **1**) and C (i.e. **3**), this implies that the dopant **2** may be suffered from its lowest tendency in forming the aligned ππ-stacking which is needed for balanced carrier transport. On the other hand, the higher current densities of devices A and C suggested the higher endurance for stressed biasing for the Pt(II) dopants **1** and **3**. The peak efficiencies of device B were recorded to be 8.5%, 14.2 cd·A^{-1}, and 12.2 lm·W^{-1}. In contrast, device A exhibited higher efficiencies of 10.0%, 20.0 cd·A^{-1} and 12.1 lm·W^{-1} at the practical brightness of 10^{2} cd·m^{-2}; while device C exhibited moderate performances: 10.0%, 16.4 cd·A^{-1} and 7.4 lm·W^{-1}. Moreover, the max. efficiencies of devices A and C reached 11.5% (23.2 cd·A^{-1}, 22.8 lm·W^{-1}) and 11.2% (18.3·cd·A^{-1}, 11.6 lm·W^{-1}), respectively. The PLQY values of **1** and **3** in the CBP host were recorded to be 58.4%, and 43.9%, respectively. This suggested the achievement of a nearly unitary internal quantum efficiency and good carrier balance in both devices.[34]

To further investigate the possible aggregation effect of these Pt(II) dopants, we also varied the doping concentration of **3** from 8 wt.% to 100 wt.% (i.e. neat film). The corresponding EL spectra are shown in Figure 9(e), with a gradual shifting of emission peak maxima to the longer wavelengths as concentration increased,[7b, 35]

together with a steady decrease in intensity for peaks at 573 and 615 nm. Eventually, the emission turned to a broadened and featureless band with maximum at 681 nm, which is in fully agreement with the formation of ^{3}MMLCT emission. In the meantime, the CIE coordinates of the non-doped device reached (0.679, 0.316), superimposable to the deep-red apex of NTSC. Figure 9(f) showed the dependence of efficiencies versus doping concentration. For devices at higher doping concentration, the reduced current densities as well as higher turn-on voltages indicated the lower carrier transport in EML. Since the hole and electron mobilities of CBP are comparable, the lower current density implied complex **3** possessing inferior carrier transport capabilities. Thus, the gradual decrease in efficiencies was resulting from the carrier imbalance induced by presence of excessive Pt(II) dopant.[36] Then, higher doping level caused the turn-on voltage to increase from 4.3 V to 5.6 V, and the maximum luminance to decrease from 7997 cd·m^{-2} (8 wt.%) to 1069 cd·m^{-2} (i.e. neat film), respectively.

Conclusion

In conclusion, Pt(II) complexes **1** ~ **4** with different *t*-butyl and dip substituents on isoquinolinyl pyrazolate chelates were synthesized. It allowed us to draw a correlation between the substituents, photophysics, solid-state packing and OLED performances. Among the Pt(II) complexes studied, those with the 5,7-di-*t*-butyl groups and 4-dip group (i.e. Pt(II) complexes **2** and **4**) can effectively prevent the intermolecular stacking interaction in solid state, exhibiting more-or-less identical spectra in both solution and solid state. In sharp contrast, those with 6-*t*-butyl and 6-dip substituted isoquinolinyl fragments (i.e. Pt(II) complexes **1** and **3**) are capable to exhibit notable mechanochromism under grinding and solvatochromism upon contacting with solvents. This structureless and red-shifted emission in both the solid state and PMMA matrix at higher concentrations are attributed to the population to triplet ^{3}MMLCT excited states.

Moreover, the studied Pt(II) complexes were also capable to serve as dopants of PHOLEDs. The peak efficiencies of OLEDs with Pt(II) dopants **1**, **2** and **3** were recorded to be 11.5% (23.2 cd·A^{-1}, 22.8 lm·W^{-1}), 8.5% (14.2 cd·A^{-1}, 12.2 lm·W^{-1}), and 11.2% (18.3 cd·A^{-1}, 13.6 lm·W^{-1}), respectively. In addition, the substituents of isoquinolinyl pyrazolate chelates have imposed a strong influence in the carrier transport properties and the device efficiencies, among which the performance of Pt(II) dopant **2** with 5,7-di-*t*-butyl substituents is much inferior to those with 6-*t*-butyl and 6-dip substituent (i.e. **1** and **3**). Furthermore, as exemplified by the Pt(II) dopant **3**, increase in doping concentrations have caused a significant red-shifting in emission, due to the dopant aggregation.

Experimental Section

General Procedures All solvents were dried over appropriate drying agents and distilled prior to use. Commercially available reagents were used without further purification, unless otherwise stated. All reactions were performed under a nitrogen atmosphere and monitored by using pre-coated TLC plates (0.20 mm with fluorescent indicator UV254). Mass spectra were obtained on a JEOL SX-102A instrument operating in electron impact (EI) or fast atom bombardment (FAB) mode. ^{1}H NMR spectra were recorded on a Varian Mercury-400 or an INOVA-500 instrument. Elemental analysis was carried out with a Heraeus CHN-O Rapid Elementary Analyzer.

Synthesis of [Pt(L1)$_2$] (1). To a 100 mL of reaction flask was added Pt(DMSO)$_2$Cl$_2$ (150 mg, 0.36 mmol), 6-*t*-butyl-1-(3-trifluoromethyl-1H-pyrazol-5-yl) isoquinoline (376 mg, 0.78 mmol), Na_2CO_3 (376 mg, 3.66 mmol) and 50 mL of THF. The mixture was heated to reflux overnight and excess of H_2O was added to induce precipitation. It was filtered and washed with acetone and diethyl ether to obtain a red solid (207 mg, 70%). Crystals of **1** were obtained from slow cooling of a saturated solution in

xylenes.

Spectral data of **1**: ^{1}H NMR (600 MHz, $CDCl_3$, 323 K): δ 10.53 (d, *J* = 6.0 Hz, 2 H), 8.47 (d, *J* = 12 Hz, 2 H), 7.79 ~ 7.78 (m, 4 H), 7.57 (d, *J* = 12 Hz, 2 H), 7.22 (s, 2 H), 1.45 (s, 18 H). ^{19}F NMR (600 MHz, $CDCl_3$, 323 K): δ −61.40 (s). MS [FAB], m/z 830.7, M^+. Anal. Calcd. for $C_{34}H_{30}F_6N_6Pt$: C, 49.10; H, 3.64; N, 10.10. Found: C, 48.82; H, 3.85; N, 10.16.

Selected crystal data of **1**: $C_{110}H_{100}F_{18}N_{18}Pt_3$; M = 2601.35; triclinic; space group = *P*−1; *a* = 11.0996(7), *b* = 15.0849(10), *c* = 15.1862(10) Å; α = 94.811(2), β = 99.629(2), γ = 94.980(2)°; *V* = 2484.9(3) Å^3; *Z* = 1; ρ_{calcd} = 1.738 Mg·m^{-3}; *F*(000) = 1282; crystal size = 0.30 × 0.07× 0.05 mm^3; λ(Mo-K_α) = 0.71073 Å; T = 150(2) K; μ = 4.306 mm^{-1}; 24310 reflections collected, 11405 independent reflections (R_{int} = 0.0715), restraints / parameters = 50 / 662, GOF = 1.056, final $R_1[I > 2\sigma(I)]$ = 0.0598 and wR_2(all data) = 0.1493.

Synthesis of [Pt(L2)$_2$] (2). A mixture of $Pt(DMSO)_2Cl_2$ (100 mg, 0.24 mmol), 3,5-di-*t*-butyl-1-(3-trifluoromethyl-1H-pyrazol-5-yl) isoquinoline (196 mg, 0.52 mmol) and Na_2CO_3 (250 mg, 2.42 mmol) in 50 mL of THF was refluxed overnight. The THF was evaporated and the crude product was purified by SiO_2 column chromatography using CH_2Cl_2 as eluent. Recrystallization from a mixture of CH_2Cl_2 and methanol gave an orange solid (156 mg, 70%).

Spectral data of **2**: ^{1}H NMR (400 MHz, $CDCl_3$, 298 K): δ 10.50 (d, *J* = 4.0 Hz, 2 H), 8.42 (s, 2 H), 8.17 (d, *J* = 8.0 Hz, 2 H), 7.91 (s, 2 H), 7.19 (s, 2 H), 1.64 (s, 18 H), 1.46 (s, 18 H). ^{19}F NMR (376 MHz, $CDCl_3$, 298 K): δ −60.77 (s, 6 F). MS [FAB], m/z 944.2, M^+. Anal. Calcd. for $C_{42}H_{46}F_6N_6Pt$: C, 53.44; H, 4.91; N, 8.90. Found: C, 53.08; H, 4.79; N, 8.82.

Synthesis of [Pt(L3)$_2$] (3). A mixture of $Pt(DMSO)_2Cl_2$ (100 mg, 0.24 mmol), 6-(2,6-diisopropylphenyl)-1-(3-trifluoromethyl-1H-pyrazol-5-yl) isoquinoline (220 mg,

0.52 mmol) and Na_2CO_3 (250 mg, 2.42 mmol) in 30 mL of THF was refluxed overnight. After then, excess of H_2O was added to induce precipitation. It was filtered and washed with CH_2Cl_2 and then diethyl ether to afford a purple solid (286 mg, 69%).

Spectral data of **3**: ^{1}H NMR (400 MHz, d_8-THF, 298 K): δ 10.76 (br, 2 H), 8.92 (br, 2 H), 7.92 (br, 4 H), 7.69 (br, 4 H), 7.41 (t, *J* = 8.0 Hz, 2 H), 7.31 (s, 2 H), 7.29 (s, 2 H), 2.65 (br, 4 H), 1.14 ~ 1.13 (m, 24 H). ^{19}F NMR (600 MHz, $CDCl_3$, 354 K): δ –61.3 (s). MS [FAB], m/z 1041.3, M^+. Anal. Calcd. for $C_{50}H_{46}F_6N_6Pt$: C, 57.74; H, 4.46; N, 8.08. Found: C, 57.76; H, 4.42; N, 8.23.

Synthesis of [Pt(L4)$_2$] (4). A mixture of $Pt(DMSO)_2Cl_2$ (100 mg, 0.24 mmol), 4-(2,6-diisopropylphenyl)-1-(3-trifluoromethyl-1H-pyrazol-5-yl) isoquinoline (220 mg, 0.52 mmol) and Na_2CO_3 (375 mg, 2.42 mmol) in 30 mL of THF was refluxed overnight. After then, the solvent was evaporated and the residue extracted with CH_2Cl_2 and concentrated. The residue was purified by SiO_2 column chromatography using CH_2Cl_2 as eluent. Orange crystals were obtained from a mixed solution of $CHCl_3$ and hexane (253 mg, 61%).

Spectral data of **4**: ^{1}H NMR (400 MHz, $CDCl_3$, 298 K): δ 10.69 (s, 2 H), 8.75 ~ 8.73 (m, 2 H), 7.74 ~ 7.72 (m, 4 H), 7.54 ~ 7.50 (m, 4 H), 7.37 (s, 2 H), 7.34 (d, *J* = 4.0 Hz, 4 H), 2.36 (hept, *J* = 6.3 Hz, 4 H), 1.09 (d, *J* = 6.7 Hz, 12 H), 0.99 (d, *J* = 6.8 Hz, 12 H). ^{19}F NMR (376 MHz, $CDCl_3$, 298 K): δ –61.52 (s). MS [FAB], m/z 1040.1, M^+. Anal. Calcd. for $C_{50}H_{46}F_6N_6Pt$: C, 57.74; H, 4.46; N, 8.08. Found: C, 57.79; H, 4.67; N, 8.27.

Selected crystal data of **4**: $C_{50}H_{46}F_6N_6Pt$; M = 1040.02; triclinic; space group = *P*–1; *a* = 8.8284(11), *b* = 9.0348(11), *c* = 14.3205(18) Å; α = 96.191(2), β = 105.828(2), γ = 90.578(2)°; *V* = 1091.6(2) Å^3; *Z* = 1; ρ_{calcd} = 1.582 Mg·m^{-3}; *F*(000) = 520; crystal size = 0.12 × 0.12× 0.05 mm^3; λ(Mo-K$_\alpha$) = 0.71073 Å; T = 150(2) K; μ = 3.282 mm^{-1}; 13773 reflections collected, 5007 independent reflections (R_{int} = 0.0585), restraints / parameters = 32 / 302, GOF = 1.083, final $R_1[I > 2\sigma(I)]$ = 0.0373 and wR_2(all data) = 0.0924.

X-ray Crystallography. All single-crystal X-ray diffraction data were measured on a Bruker Smart CCD diffractometer using λ (Mo Kα) radiation (λ = 0.71073 Å). The data collection was executed using the SMART program. Cell refinement and data reduction were made with the SAINT program. The structure was determined using the SHELXTL/PC program and refined using full matrix least-squares.[37] All non-hydrogen atoms were refined anisotropically, whereas hydrogen atoms were placed at the calculated positions and included in the final stage of refinements with fixed parameters. CCDC 1026840 and 1026841 contain the supplementary crystallographic data for this paper. These data can be obtained free of charge from the Cambridge Crystallographic Data Centre via www.ccdc.cam.ac.uk/data request/cif.

OLED Fabrication. All commercial materials were purchased from Nichem and Lumtec, and were subjected to temperature-gradient sublimation under high vacuum before use. The ITO glasses with a sheet resistance of ~15 Ω/square were washed with detergent solution and treated with UV-ozone to increase the work function. The OLED architecture consists of multiple organic layers and reflective cathode which were consecutively deposited onto the ITO by thermal evaporation in a chamber with a base pressure of < 10^{-6} torr without breaking the vacuum. The deposition rates of organics and aluminum were kept at around 0.1 nm/s and 0.5 nm/s, respectively. The active area was defined by the shadow mask (2 × 2 mm^2). Current density-voltage-luminance characterization was measured using a Keithley 238 current source-measure unit and a Keithley 6485 picoammeter equipped with a calibrated Si-photodiode. The electroluminescent spectra were recorded using an Ocean Optics spectrometer.

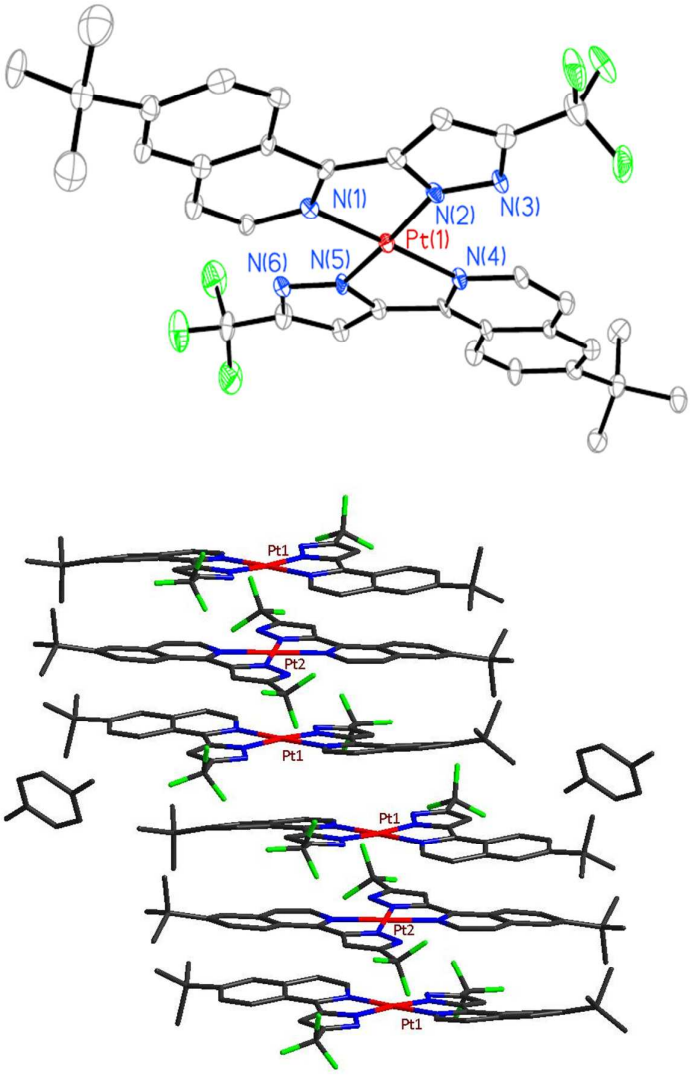

Figure 1. (a) Structural drawing of **1** with thermal ellipsoids shown at 40% probability level, selected bond distances: Pt(1)-N(1) = 2.041(7), Pt(1)-N(2) = 2.010(7), Pt(1)-N(4) = 2.033(7), Pt(1)-N(5) = 2.009(7) Å; selected bond angles: N(1)-Pt-N(2) = 78.7(3), N(1)-Pt-N(4) = 178.6(3), N(2)-Pt-N(5) = 175.8(3) and N(4)-Pt-N(5) = 78.5(3)°. (b) Packing diagrams of trimeric **1**·xylenes with nonbonding interactions Pt1···Pt2 = 3.338 Å and Pt1···Pt1 = 5.197 Å.

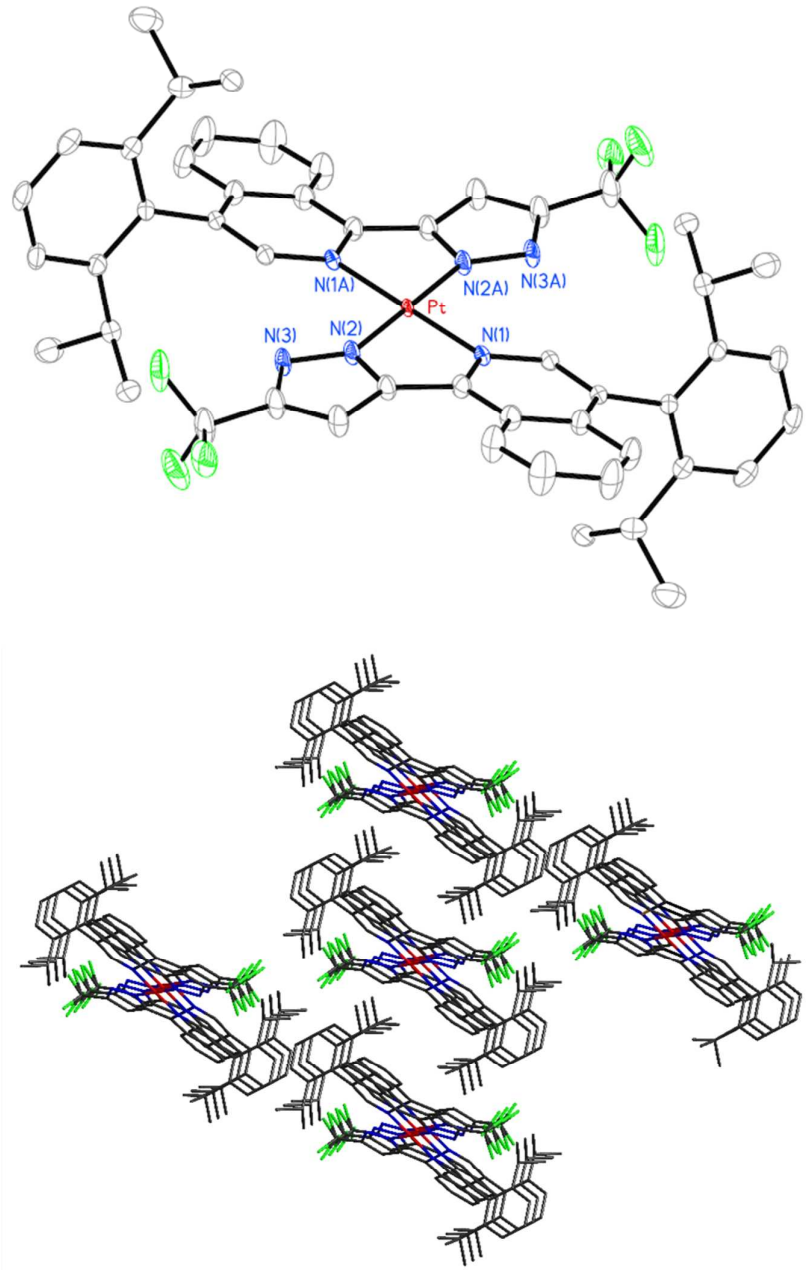

Figure 2. (a) Structural drawing of **4** with thermal ellipsoids shown at 40% probability level, selected bond distances: Pt(1)-N(1) = 2.040(4), Pt(1)-N(2) = 1.998(4) and N(2)-N(3) = 1.346(5) Å; selected bond angles: N(1)-Pt-N(2) = 78.15(16), N(1)-Pt-N(1A) = 180.0(3), N(2)-Pt-N(2A) = 180.0(3) and N(1)-Pt-N(2A) = 101.85(16)°. (b) Packing diagrams of planar platinum(II) complexes of **4**. Parallel stacking arrangement of **4** with the shortest Pt···Pt contact of 8.828 Å.

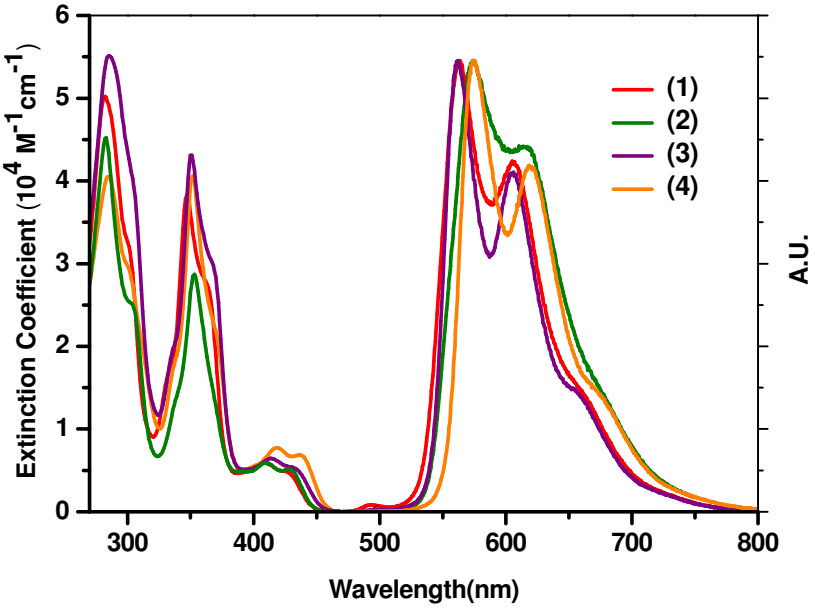

Figure 3. UV-Vis absorption spectra and solution state emission spectra in CH_2Cl_2 of Pt(II) complexes **1**, **2**, **3** and **4**.

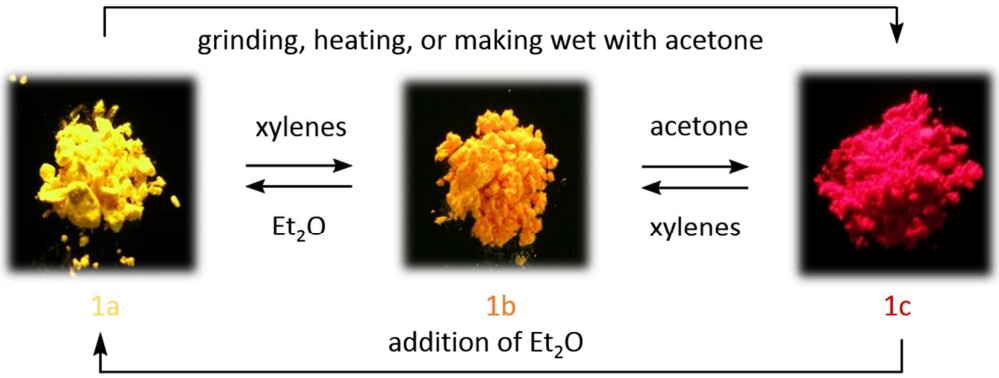

Figure 4. Interconversion between three kind of solid samples of **1**, among which yellow **1a**, orange **1b** and red **1c** were obtained by making wet with diethyl ether, xylenes, and acetone, respectively. Photographs were taken under (365 nm) UV irradiation.

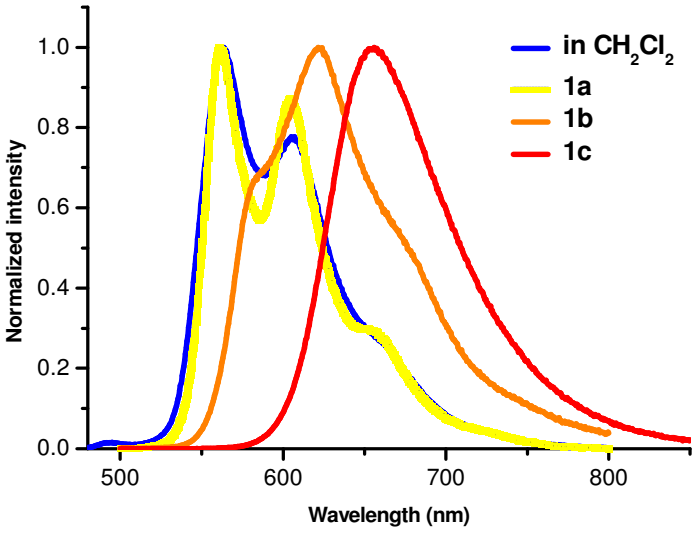

Figure 5. Emission spectral of solid samples of **1a**, **1b** and **1c** and in CH_2Cl_2 solution at conc. of 10^{-5} M.

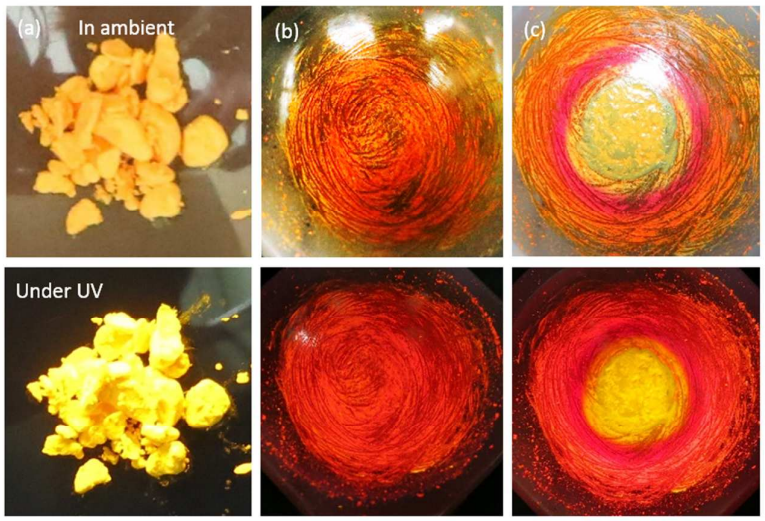

Figure 6. Photographic images of color and luminescence changes of complex **1** in response to mechanical grinding and solvent treatment: (a) unground sample, (b) ground sample, and (c) making wet with diethyl ether. Photographs were taken under ambient light and UV irradiation (365 nm).

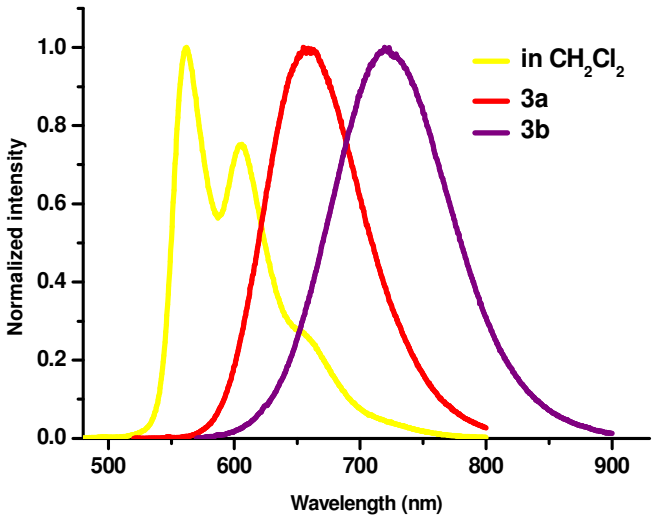

Figure 7. Emission spectral of solid samples of **3a** and **3b**, obtained by making wet with diethyl ether and THF, respectively, and spectrum recorded in CH_2Cl_2 at conc. of 10^{-5} M.

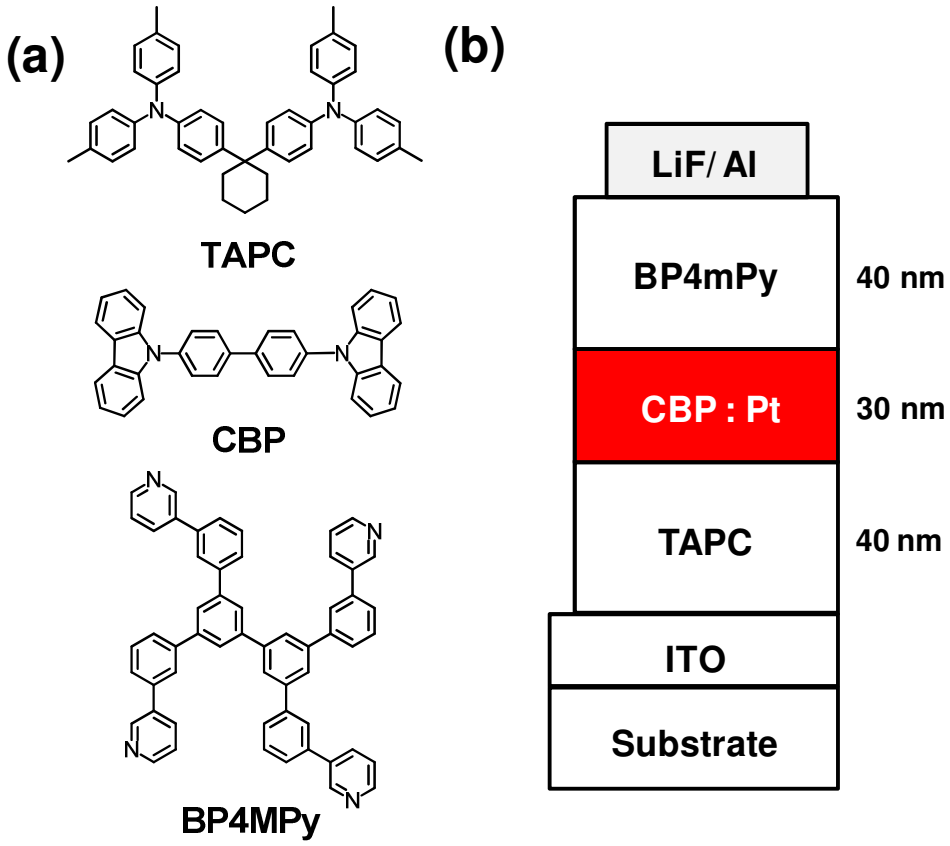

Figure 8. (a) Chemical structure of the materials used; (b) schematic structures of the tested OLEDs.

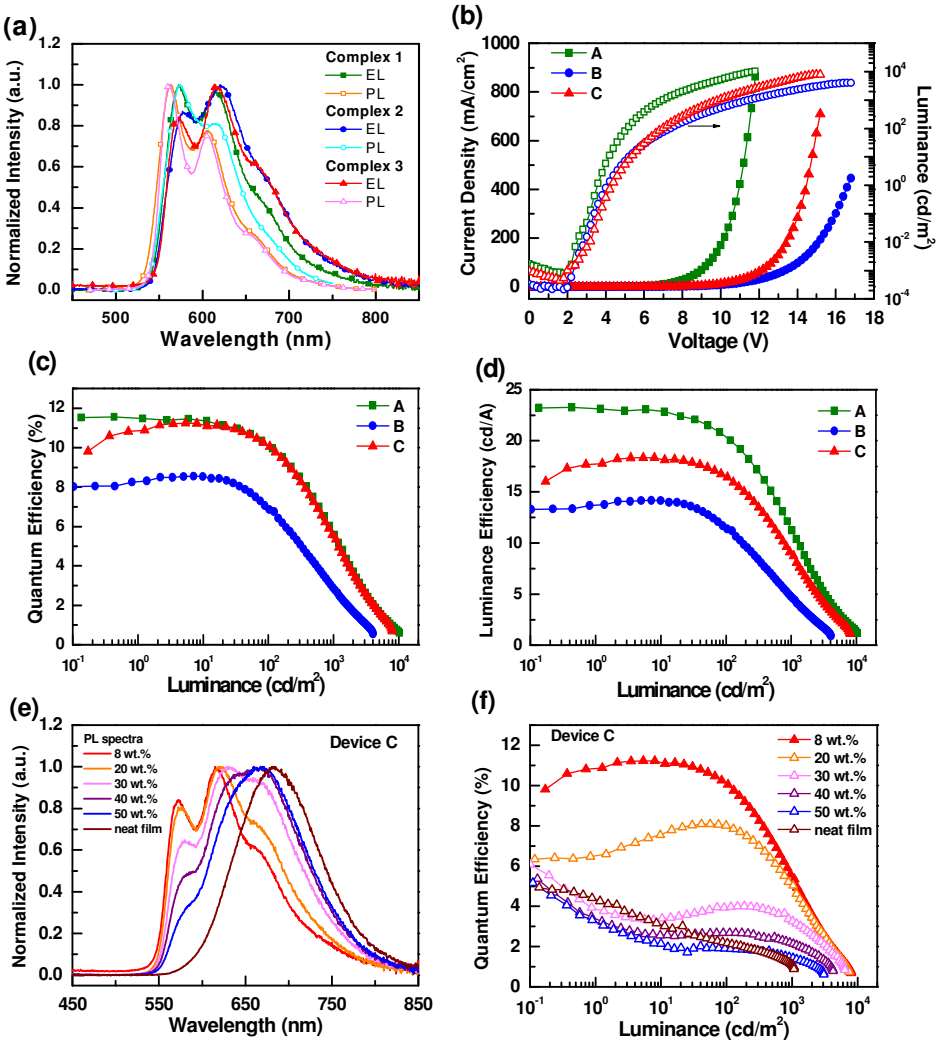

Figure 9. EL characteristics of Devices A, B, and C for complexes **1**, **2**, and **3**. (a) PL and EL spectra of complexes **1**, **2** and **3** indicated as devices A, B and C, respectively. (b) current density–voltage–luminance (*J*-*V*-*L*) plots; (c) external quantum efficiency vs. luminance plots; (d) luminance efficiency vs. luminance plots for devices A, B and C. (e) EL spectra of device C with different doping concentrations; (f) external quantum efficiency vs. luminance plots of device C with different doping concentrations.

Table 1 UV-Vis absorption and emission data of Pt(II) phosphors.

	Abs λ /nm ($\varepsilon \times 10^{-4}$ M^{-1} cm^{-1})[a]	Em $\lambda_{(max)}$ (nm)[a]	τ_{obs} (μs)[a]	Φ (%)[a]	k_r (s^{-1}) [b]	k_{nr} (s^{-1}) [c]
1	282 (5.02), 347 (3.83), 364 (2.71), 409 (0.59), 428 (0.47)	564, 605, 663 (sh)	15.5	32	2.06×10^4	4.39×10^4
2	283 (4.52), 353 (2.87), 409 (0.59), 429 (0.51)	575, 617, 676 (sh)	17.7	21	1.19×10^4	4.47×10^4
3	285 (5.52), 350 (4.31), 368 (2.98), 414 (0.64), 433 (0.52)	562, 606, 655 (sh)	22.0	34	1.54×10^4	2.99×10^4
4	285 (4.05), 347 (3.83), 418 (0.77), 438 (0.68)	574, 620, 676 (sh)	26.1	20	7.66×10^3	3.06×10^4

[a] UV-Vis spectra, photoluminescence spectra, lifetime and quantum yields were recorded in CH_2Cl_2 at conc. of 10^{-5} M. 4-(Dicyanomethylene)-2-methyl-6-(4-dimethylaminostyryl)-4*H*-pyran in ethanol as the reference standard ($\Phi = 0.435$).

[b] $(k_r + k_{nr}) = 1 / \tau_{obs}$ where τ_{obs} is the emission lifetime.

[c] The radiative decay rate constant kr is calculated by Φ (%) = $k_r / (k_r + k_{nr})$.

Table 2. EL characteristics of tested OLEDs with different Pt(II) dopants.

Device		A	B	C
dopant (8 wt.%)		**1**	**2**	**3**
External Quantum Efficiency (%)	[a]	11.5	8.5	11.2
	[b]	10.0	6.8	10.0
Luminescence Efficiency (cd/A)	[a]	23.2	14.2	18.3
	[b]	20.0	11.3	16.4
Power Efficiency (lm/W)	[a]	22.8	12.2	13.6
	[b]	12.1	4.8	7.4
V_{on} (V)	[c]	3.6	4.1	4.3
Max. Luminance (cd/m^2) [Voltage]		10318 [11.8 V]	4052 [16.8 V]	7997 [15.2 V]
CIE 1931 coordinates	[b]	(0.563, 0.434)	(0.578, 0.419)	(0.579, 0.417)
	[d]	(0.562, 0.435)	(0.574, 0.415)	(0.575, 0.416)

[a] maximum efficiency; [b] recorded at 10^2 cd/m^2; [c] turn-on voltage measured at 1 cd/m^2; [d] measured at 10^3 cd/m^2.

Table 3. The full width at half maximum (FWHM) and emission peaks extracted from the PL spectra and EL spectra of Pt(II) dopants **1** ~ **3**.

Pt dopant	PL spectrum (in CH_2Cl_2)		EL spectrum	
	FWHM (nm)	peak max. (nm)	FWHM (nm)	peak max. (nm)
1	81	564, 605	100	573, 614.5
2	89	575, 617	120	577, 620.5
3	74	562, 606	121	572.5, 615

References

1. (a) Y. Chi, B. Tong and P.-T. Chou, *Coord. Chem. Rev.*, 2014, **281**, 1; (b) H. Xiang, J. Cheng, X. Ma, X. Zhou and J. J. Chruma, *Chem. Soc. Rev.*, 2013, **42**, 6128; (c) G. Zhou, W.-Y. Wong and X. Yang, *Chem. Asian J.*, 2011, **6**, 1706; (d) L. Xiao, Z. Chen, B. Qu, J. Luo, S. Kong, Q. Gong and J. Kido, *Adv. Mater.*, 2011, **23**, 926; (e) Y. Chi and P.-T. Chou, *Chem. Soc. Rev.*, 2010, **39**, 638; (f) Y. You and S. Y. Park, *Dalton Trans.*, 2009, 1267; (g) R. C. Evans, P. Douglas and C. J. Winscom, *Coord. Chem. Rev.*, 2006, **250**, 2093.
2. (a) B. Minaev, G. Baryshnikov and H. Agren, *Phys. Chem. Chem. Phys.*, 2014, **16**, 1719; (b) W. C. H. Choy, W. K. Chan and Y. Yuan, *Adv. Mater.*, 2014, **26**, 5368; (c) H. Sasabe and J. Kido, *J. Mater. Chem. C*, 2013, **1**, 1699; (d) P.-T. Chou, Y. Chi, M.-W. Chung and C.-C. Lin, *Coord. Chem. Rev.*, 2011, **255**, 2653; (e) W.-Y. Wong and C.-L. Ho, *J. Mater. Chem.*, 2009, **19**, 4457; (f) P.-T. Chou and Y. Chi, *Chem. Eur. J.*, 2007, **13**, 380.
3. (a) C. Fan and C. Yang, *Chem. Soc. Rev.*, 2014, **43**, 6439; (b) J. Kalinowski, V. Fattori, M. Cocchi and J. A. G. Williams, *Coord. Chem. Rev.*, 2011, **255**, 2401; (c) K. M.-C. Wong and V. W.-W. Yam, *Acc. Chem. Res.*, 2011, **44**, 424; (d) A. Diez, E. Lalinde and M. T. Moreno, *Coord. Chem. Rev.*, 2011, **255**, 2426; (e) J. A. G. Williams, *Chem. Soc. Rev.*, 2009, **38**, 1783; (f) J. A. G. Williams, S. Develay, D. L. Rochester and L. Murphy, *Coord. Chem. Rev.*, 2008, **252**, 2596.
4. (a) A. Amar, H. Meghezzi, J. Boixel, H. Le Bozec, V. Guerchais, D. Jacquemin and A. Boucekkine, *J. Phys. Chem. A*, 2014, **118**, 6278; (b) Y. Abe, Y. Takagi, M. Nakamura, T. Takeuchi, T. Tanase, M. Yokokawa, H. Mukai, T. Megumi, A. Hachisuga and K. Ohta, *Inorg. Chim. Acta*, 2012, **392**, 254; (c) A. Diez, J. Fornies, C. Larraz, E. Lalinde, J. A. Lopez, A. Martin, M. T. Moreno and V. Sicilia, *Inorg. Chem.*, 2010, **49**, 3239; (d) K. M.-C. Wong, C.-K. Hui, K.-L. Yu and V. W.-W. Yam, *Coord. Chem. Rev.*, 2002, **229**, 123; (e) V. M. Miskowski and V. H. Houlding, *Inorg. Chem.*, 1991, **30**, 4446; (f) E. Rossi, A. Colombo, C. Dragonetti, D. Roberto, F. Demartin, M. Cocchi, P. Brulatti, V. Fattori and J. A. G. Williams, *Chem. Commun.*, 2012, **48**, 3182.
5. (a) M. Han, Y. Tian, Z. Yuan, L. Zhu and B. Ma, *Angew. Chem. Int. Ed.*, 2014, in press; (b) T. Fleetham, J. Ecton, Z. Wang, N. Bakken and J. Li, *Adv. Mater.*, 2013, **25**, 2573; (c) E. S.-H. Lam, D. P.-K. Tsang, W. H. Lam, A. Y.-Y. Tam, M.-Y. Chan, W.-T. Wong and V. W.-W. Yam, *Chem. Eur. J.*, 2013, **19**, 6385; (d) L. Murphy, P. Brulatti, V. Fattori, M. Cocchi and J. A. G. Williams, *Chem. Commun.*, 2012, **48**,

5817; (e) W. Mroz, C. Botta, U. Giovanella, E. Rossi, A. Colombo, C. Dragonetti, D. Roberto, R. Ugo, A. Valore and J. A. G. Williams, *J. Mater. Chem.*, 2011, **21**, 8653; (f) J. Kalinowski, M. Cocchi, L. Murphy, J. A. G. Williams and V. Fattori, *Chem. Phys.*, 2010, **378**, 47; (g) M. Cocchi, J. Kalinowski, D. Virgili, V. Fattori, S. Develay and J. A. G. Williams, *Appl. Phys. Lett.*, 2007, **90**, 163508.

6. (a) G. Li, T. Fleetham and J. Li, *Adv. Mater.*, 2014, **26**, 2931; (b) G. Cheng, S. C. F. Kui, W.-H. Ang, M.-Y. Ko, P.-K. Chow, C.-L. Kwong, C.-C. Kwok, C. Ma, X. Guan, K.-H. Low, S.-J. Su and C.-M. Che, *Chem. Sci.*, 2014, **5**, 4819; (c) S.-L. Lai, W.-Y. Tong, S. C. F. Kui, M.-Y. Chan, C.-C. Kwok and C.-M. Che, *Adv. Funct. Mater.*, 2013, **23**, 5168; (d) S. C. F. Kui, P. K. Chow, G. S. M. Tong, S.-L. Lai, G. Cheng, C.-C. Kwok, K.-H. Low, M. Y. Ko and C.-M. Che, *Chem. Eur. J.*, 2013, **19**, 69; (e) E. Turner, N. Bakken and J. Li, *Inorg. Chem.*, 2013, **52**, 7344; (f) J. Zhang, F. Zhao, X. Zhu, W.-K. Wong, D. Ma and W.-Y. Wong, *J. Mater. Chem.*, 2012, **22**, 16448; (g) D. A. K. Vezzu, J. C. Deaton, J. S. Jones, L. Bartolotti, C. F. Harris, A. P. Marchetti, M. Kondakova, R. D. Pike and S. Huo, *Inorg. Chem.*, 2010, **49**, 5107.

7. (a) J. Kavitha, S.-Y. Chang, Y. Chi, J.-K. Yu, Y.-H. Hu, P.-T. Chou, S.-M. Peng, G.-H. Lee, Y.-T. Tao, C.-H. Chien and A. J. Carty, *Adv. Funct. Mater.*, 2005, **15**, 223; (b) S.-Y. Chang, J. Kavitha, S.-W. Li, C.-S. Hsu, Y. Chi, Y.-S. Yeh, P.-T. Chou, G.-H. Lee, A. J. Carty, Y.-T. Tao and C.-H. Chien, *Inorg. Chem.*, 2005, **45**, 137.

8. (a) X. Wang, Y.-L. Chang, J.-S. Lu, T. Zhang, Z.-H. Lu and S. Wang, *Adv. Funct. Mater.*, 2014, **24**, 1911; (b) C. Cebrian, M. Mauro, D. Kourkoulos, P. Mercandelli, D. Hertel, K. Meerholz, C. A. Strassert and L. De Cola, *Adv. Mater.*, 2013, **25**, 437; (c) S.-Y. Chang, J.-L. Chen, Y. Chi, Y.-M. Cheng, G.-H. Lee, C.-M. Jiang and P.-T. Chou, *Inorg. Chem.*, 2007, **46**, 11202; (d) S.-Y. Chang, Y.-M. Cheng, Y. Chi, Y.-C. Lin, C.-M. Jiang, G.-H. Lee and P.-T. Chou, *Dalton Trans.*, 2008, 6901; (e) C.-T. Liao, H.-H. Chen, H.-F. Hsu, A. Poloek, H.-H. Yeh, Y. Chi, K.-W. Wang, C.-H. Lai, G.-H. Lee, C.-W. Shih and P.-T. Chou, *Chem. Eur. J.*, 2011, **17**, 546.

9. (a) Q. Wang, I. W. H. Oswald, X. Yang, G. Zhou, H. Jia, Q. Qiao, Y. Chen, J. Hoshikawa-Halbert and B. E. Gnade, *Adv. Mater.*, 2014, in press; (b) Q. Wang, I. W. H. Oswald, M. R. Perez, H. Jia, A. A. Shahub, Q. Qiao, B. E. Gnade and M. A. Omary, *Adv. Funct. Mater.*, 2014, **24**, 4746-4752; (c) L.-M. Huang, G.-M. Tu, Y. Chi, W.-Y. Hung, Y.-C. Song, M.-R. Tseng, P.-T. Chou, G.-H. Lee, K.-T. Wong, S.-H. Cheng and W.-S. Tsai, *J. Mater. Chem. C*, 2013, **1**, 7582.

10. (a) S.-Y. Chang, J. Kavitha, J.-Y. Hung, Y. Chi, Y.-M. Cheng, E. Y. Li, P.-T. Chou, G.-H. Lee and A. J. Carty, *Inorg. Chem.*, 2007, **46**, 7064; (b) K.-L. Wu, W.-P. Ku, J. N. Clifford, E. Palomares, S.-T. Ho, Y. Chi, S.-H. Liu, P.-T. Chou, M. K.

Nazeeruddin and M. Grätzel, *Energy Environ. Sci.*, 2013, **6**, 859; (c) C.-C. Chou, F.-C. Hu, H.-H. Yeh, H.-P. Wu, Y. Chi, J. N. Clifford, E. Palomares, S.-H. Liu, P.-T. Chou and G.-H. Lee, *Angew. Chem. Int. Ed.*, 2014, **53**, 178.

11. (a) A. L. Smith, F. F. De Morin, N. A. Paras, Q. Huang, J. K. Petkus, E. M. Doherty, T. Nixey, J. L. Kim, D. A. Whittington, L. F. Epstein, M. R. Lee, M. J. Rose, C. Babij, M. Fernando, K. Hess, Q. Le, P. Beltran and J. Carnahan, *J. Med. Chem.*, 2009, **52**, 6189; (b) J. B. Hendrickson and C. Rodriguez, *J. Org. Chem.*, 1983, **48**, 3344.
12. C. Giordano, F. Minisci, E. Vismara and S. Levi, *J. Org. Chem.*, 1986, **51**, 536.
13. M.-W. Chung, T.-Y. Lin, C.-C. Hsieh, K.-C. Tang, H. Fu, P.-T. Chou, S.-H. Yang and Y. Chi, *J. Phys. Chem. A*, 2010, **114**, 7886.
14. (a) B.-S. Du, J.-L. Liao, M.-H. Huang, C.-H. Lin, H.-W. Lin, Y. Chi, H.-A. Pan, G.-L. Fan, K.-T. Wong, G.-H. Lee and P.-T. Chou, *Adv. Funct. Mater.*, 2012, **22**, 3491; (b) S.-W. Li, Y.-M. Cheng, Y.-S. Yeh, C.-C. Hsu, P.-T. Chou, S.-M. Peng, G.-H. Lee, Y.-L. Tung, P.-C. Wu, Y. Chi, F.-I. Wu and C.-F. Shu, *Chem. Eur. J.*, 2005, **11**, 6347.
15. H.-Y. Hsieh, C.-H. Lin, G.-M. Tu, Y. Chi and G.-H. Lee, *Inorg. Chim. Acta*, 2009, **362**, 4734.
16. H. Li, J. Li, J. Ding, W. Yuan, Z. Zhang, L. Zou, X. Wang, H. Zhan, Z. Xie, Y. Cheng and L. Wang, *Inorg. Chem.*, 2014, **53**, 810-821.
17. L. Holland, W.-Z. Shen, P. von Grebe, P. J. Sanz Miguel, F. Pichierri, A. Springer, C. A. Schalley and B. Lippert, *Dalton Trans.*, 2011, **40**, 5159.
18. (a) Y.-S. Yeh, Y.-M. Cheng, P.-T. Chou, G.-H. Lee, C.-H. Yang, Y. Chi, C.-F. Shu and C.-H. Wang, *ChemPhysChem*, 2006, **7**, 2294; (b) K. Chen, C.-H. Yang, Y. Chi, C.-S. Liu, C.-H. Chang, C.-C. Chen, C.-C. Wu, M.-W. Chung, Y.-M. Cheng, G.-H. Lee and P.-T. Chou, *Chem. Eur. J.*, 2010, **16**, 4315; (c) S.-H. Chang, C.-F. Chang, J.-L. Liao, Y. Chi, D.-Y. Zhou, L.-S. Liao, T.-Y. Jiang, T.-P. Chou, E. Y. Li, G.-H. Lee, T.-Y. Kuo and P.-T. Chou, *Inorg. Chem.*, 2013, **52**, 5867.
19. (a) A. M. Prokhorov, T. Hofbeck, R. Czerwieniec, A. F. Suleymanova, D. N. Kozhevnikov and H. Yersin, *J. Am. Chem. Soc.*, 2014, **136**, 9637; (b) D. M. Jenkins, J. F. Senn and S. Bernhard, *Dalton Trans.*, 2012, **41**, 8077.
20. W. Sotoyama, T. Satoh, H. Sato, A. Matsuura and N. Sawatari, *J. Phys. Chem. A*, 2005, **109**, 9760.
21. R. E. Harding, S.-C. Lo, P. L. Burn and I. D. W. Samuel, *Org. Electron.*, 2008, **9**, 377.
22. (a) M. Hissler, W. B. Connick, D. K. Geiger, J. E. McGarrah, D. Lipa, R. J. Lachicotte and R. Eisenberg, *Inorg. Chem.*, 2000, **39**, 447; (b) M. Kato, A. Omura, A. Toshikawa, S. Kishi and Y. Sugimoto, *Angew. Chem. Int. Ed.*, 2002,

41, 3183; (c) S. A. Willison, H. Jude, R. M. Antonelli, J. M. Rennekamp, N. A. Eckert, J. A. K. Bauer and W. B. Connick, *Inorg. Chem.*, 2004, **43**, 2548; (d) F. Hua, S. Kinayyigit, J. R. Cable and F. N. Castellano, *Inorg. Chem.*, 2005, **44**, 471; (e) I. M. Sluch, A. J. Miranda, O. Elbjeirami, M. A. Omary and L. M. Slaughter, *Inorg. Chem.*, 2012, **51**, 10728.

23. X. Zhang, Z. Chi, Y. Zhang, S. Liu and J. Xu, *J. Mater. Chem. C*, 2013, **1**, 3376.
24. (a) T. Abe, T. Itakura, N. Ikeda and K. Shinozaki, *Dalton Trans.*, 2009, 711; (b) J. Ni, X. Zhang, Y.-H. Wu, L.-Y. Zhang and Z.-N. Chen, *Chem. Eur. J.*, 2011, **17**, 1171; (c) Y. Nishiuchi, A. Takayama, T. Suzuki and K. Shinozaki, *Eur. J. Inorg. Chem.*, 2011, 1815; (d) X. Zhang, J.-Y. Wang, J. Ni, L.-Y. Zhang and Z.-N. Chen, *Inorg. Chem.*, 2012, **51**, 5569; (e) J. R. Kumpfer, S. D. Taylor, W. B. Connick and S. J. Rowan, *J. Mater. Chem.*, 2012, **22**, 14196; (f) Y. Chen, W. Lu and C.-M. Che, *Organometallics*, 2013, **32**, 350; (g) T. Ohba, A. Kobayashi, H.-C. Chang and M. Kato, *Dalton Trans.*, 2013, **42**, 5514; (h) M. Krikorian, S. Liu and T. M. Swager, *J. Am. Chem. Soc.*, 2014, **136**, 2952; (i) J. Ni, Y.-G. Wang, H.-H. Wang, L. Xu, Y.-Q. Zhao, Y.-Z. Pan and J.-J. Zhang, *Dalton Trans.*, 2014, **43**, 352.
25. P. Brulatti, V. Fattori, S. Muzzioli, S. Stagni, P. P. Mazzeo, D. Braga, L. Maini, S. Milita and M. Cocchi, *J. Mater. Chem. C*, 2013, **1**, 1823.
26. (a) X. Ren, J. Li, R. J. Holmes, P. I. Djurovich, S. R. Forrest and M. E. Thompson, *Chem. Mater.*, 2004, **16**, 4743; (b) S.-J. Su, H. Sasabe, T. Takeda and J. Kido, *Chem. Mater.*, 2008, **20**, 1691.
27. (a) W.-Y. Hung, L.-C. Chi, W.-J. Chen, Y.-M. Chen, S.-H. Chou and K.-T. Wong, *J. Mater. Chem.*, 2010, **20**, 10113; (b) C.-H. Chang, M.-C. Kuo, W.-C. Lin, Y.-T. Chen, K.-T. Wong, S.-H. Chou, E. Mondal, R. C. Kwong, S. Xia, T. Nakagawa and C. Adachi, *J. Mater. Chem.*, 2012, **22**, 3832; (c) C.-H. Chang, Z.-J. Wu, Y.-H. Liang, Y.-S. Chang, C.-H. Chiu, C.-W. Tai and H.-H. Chang, *Thin Solid Films*, 2013, **548**, 389.
28. J. Kalinowski, M. Cocchi, V. Fattori, L. Murphy and J. A. G. Williams, *Org. Electron.*, 2010, **11**, 724.
29. (a) H. Matsushima, S. Naka, H. Okada and H. Onnagawa, *Curr. Appl. Phys.*, 2005, **5**, 305; (b) M. H. Tsai, Y. H. Hong, C. H. Chang, H. C. Su, C. C. Wu, A. Matoliukstyte, J. Simokaitiene, S. Grigalevicius, J. V. Grazulevicius and C. P. Hsu, *Adv. Mater.*, 2007, **19**, 862.
30. (a) K. Goushi, R. Kwong, J. J. Brown, H. Sasabe and C. Adachi, *J. Appl. Phys.*, 2004, **95**, 7798; (b) J. Lee, N. Chopra, S.-H. Eom, Y. Zheng, J. Xue, F. So and J. Shi, *Appl. Phys. Lett.*, 2008, **93**, 123306.
31. S.-J. Su, D. Tanaka, Y.-J. Li, H. Sasabe, T. Takeda and J. Kido, *Org. Lett.*, 2008, **10**,

941.

32. D. Curiel, M. Mas-Montoya, C.-H. Chang, P.-Y. Chen, C.-W. Tai and A. Tarraga, *J. Mater. Chem. C*, 2013, **1**, 3421.
33. C.-H. Chang, C.-C. Chen, C.-C. Wu, C.-H. Yang and Y. Chi, *Org. Electron.*, 2009, **10**, 1364.
34. Y. Kawamura, H. Sasabe and C. Adachi, *J. J. Appl. Phys.*, 2004, **43**, 7729.
35. Y.-H. Song, S.-J. Yeh, C.-T. Chen, Y. Chi, C.-S. Liu, J.-K. Yu, Y.-H. Hu, P.-T. Chou, S.-M. Peng and G.-H. Lee, *Adv. Funct. Mater.*, 2004, **14**, 1221.
36. (a) H. Aziz and Z. D. Popovic, *Appl. Phys. Lett.*, 2002, **80**, 2180; (b) C.-H. Chang, K.-C. Tien, C.-C. Chen, M.-S. Lin, H.-C. Cheng, S.-H. Liu, C.-C. Wu, J.-Y. Hung, Y.-C. Chiu and Y. Chi, *Org. Electron.*, 2010, **11**, 412.
37. G. M. Sheldrick, *Acta Crystallogr., Sect. A: Found. Crystallogr.*, 2008, **64**, 112.

TOC Illustration:

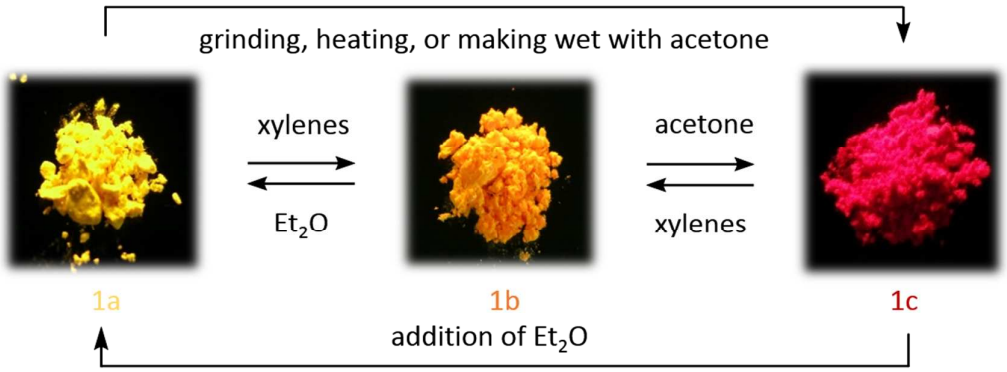

Pt(II) complex $[Pt(Lx)_2]$, L*x*H = 6-***t*-butyl**-1-(3-trifluoromethyl-1H-pyrazol-5-yl) isoquinoline, with three colored morphologies can be interconverted by grinding and/or making wet with solvents.